



HAL
open science

Indoor thermal behaviour of an office equipped with a ventilated slab: a numerical study

Matthieu Labat, Ion Hazyuk, Matthieu Cezard, Sylvie Lorente

► To cite this version:

Matthieu Labat, Ion Hazyuk, Matthieu Cezard, Sylvie Lorente. Indoor thermal behaviour of an office equipped with a ventilated slab: a numerical study. *Journal of Building Performance Simulation*, 2021, 14 (3), pp.227-246. 10.1080/19401493.2021.1905714 . hal-03196288

HAL Id: hal-03196288

<https://hal.insa-toulouse.fr/hal-03196288>

Submitted on 12 Apr 2021

HAL is a multi-disciplinary open access archive for the deposit and dissemination of scientific research documents, whether they are published or not. The documents may come from teaching and research institutions in France or abroad, or from public or private research centers.

L'archive ouverte pluridisciplinaire **HAL**, est destinée au dépôt et à la diffusion de documents scientifiques de niveau recherche, publiés ou non, émanant des établissements d'enseignement et de recherche français ou étrangers, des laboratoires publics ou privés.

Indoor thermal behavior of an office equipped with a ventilated slab: a numerical study

Matthieu Labat*¹, Ion Hazyuk², Matthieu Cezard^{1,3}, Sylvie Lorente^{1,4}

¹LMDC, INSA/UPS Génie Civil, 135 Avenue de Rangueil, 31077 Toulouse cedex 04 France.

²Institut Clément Ader, Université de Toulouse, INSA/ISAE-SUPAERO/MINES-ALBI/UPS/CNRS, 31400 Toulouse, France

³IC Entreprises, Immeuble Le Volta – 17/19 rue Jeanne Braconnier - 92360 MEUDON LA FORET

⁴Villanova University, Department of Mechanical Engineering, Villanova, PA 19085, USA

*Corresponding author: m_labat@insa-toulouse.fr

Abstract

Ventilated slabs are used to provide indoor comfort by taking advantage of thermal inertia. The underlying difficulty is that the computational cost is high, which is hardly compatible with an exhaustive study of dynamic behavior at room scale. This paper presents a methodology for obtaining a lumped model based on the identification of the transfer functions for constant airflow rate systems. The transfer functions were combined into a state space model, which is able to obtain the main heat fluxes with good accuracy at a much lower computational cost. The study moved to room scale in order to further understand how a ventilated slab influences the heat balance. Increasing the number of ducts promoted better indoor temperature stability but the impact was slight. The mass flow rate, on the other hand, appeared to be crucial. This result underlines the need to tailor a control law specifically to the ventilated slab.

Keywords:

TABS, ventilated slab, state space model, thermal inertia

Nomenclature

Latin Symbols	Description	Unit
A	Area	m^2
C_p	Specific heat capacity	$J.kg^{-1}.K^{-1}$
d	Diameter	m
f	Frequency	s^{-1}
f_D	Darcy friction factor	-
E	Energy consumption	J
F	Transfer function	
H	Thickness of the slab	m
h	Convective heat transfer coefficient	$W.m^{-2}.K^{-1}$
k	Thermal conductivity	$W.m^{-1}.K^{-1}$
K	Static gain	
L	Length of the slab	m
P	Period	s
p_d	Perimeter of the duct cross-section	m
p	Pole of a transfer function	s
\dot{Q}	Heat flux	W
\dot{m}	Mass flow rate	$kg.s^{-1}$
Nu	Nusselt number	-
Pr	Prandtl number	-
Re	Reynolds number	-
s	Laplace variable	-
T	Temperature	K or $^{\circ}C$
t	Time	s
U	Overall heat transfer coefficient	$W.m^{-2}.K^{-1}$
V	Volume	m^3
W	Center-to-center duct distance	m
z	Zero of a transfer function	
Greek Symbols		
α	Thermal diffusivity	$m^2.s^{-1}$
ρ	Density	$kg.m^{-3}$
τ	Time delay	s
Subscripts		
a	air	
B	Blown into the room	

<i>c</i>	concrete
<i>D</i>	ducts
<i>f</i>	floor
<i>in</i>	Inlet of the pipe
<i>L</i>	Loads
<i>s</i>	Stored
<i>T</i>	Transmitted to the room
<i>u</i>	Upper face
<i>w</i>	Wall
Upper scripts	
—	Mean value
^	Amplitude

1. Introduction

Thermally Activated Building System (TABS) are parts of building structures that are used to store energy and release it later. This denomination refers notably – but not exclusively – to concrete floors or ceilings with embedded water pipes, as exemplified in (Antonopoulos and Tzivanidis, 1997; Koschenz and Dorer, 1999; Zhang et al., 2012). TABS have been attracting the interest of researchers in recent decades (Romaní et al., 2016). The reason is to be found in the great thermal comfort they can offer while saving energy, taking advantage of the use of radiative heat transfer (Rhee et al., 2017) and high thermal inertia. While modern TABS often use water as the heat transfer fluid, mostly because it has high density and specific heat, the concept of storing heat in a building structure is quite ancient and initially used air as the medium to transport heat. It can be traced back thousands of years and has been found in multiple locations across the globe. The *huoqiang*, which consisted of baked earth, is believed to have matured and given birth to the Chinese *kang* (Bean et al., 2010). (Zhuang et al., 2009) explain that, during the 1990's, the Chinese government promoted the use of a more modern, more efficient *kang*, which is elevated and thus uses both faces for heat transfer. The Korean *ondol* is a system that is quite similar to the *kang*. It is now the prevalent heating system in Korean residential

buildings. Ancient Roman public bathhouses comprised several baths of different temperatures, heated thanks to what we call a hypocaust. (Thébert, 2003) presents several archeological sites attesting to the presence of heated public baths that prefigured the modern hypocausts. In (Basaran and Ilken, 1998), the energetic efficiency of such a system is debated. Later, in Europe, (Evelyn, 1691) described a greenhouse heated by an outside furnace with pipes running underground along the whole length of the greenhouse floor. Liverpool Cathedral used an air-based radiant heating system (Haden, 1924), where the air flowed in a closed loop.

More recently, TABS using hollow-core concrete slabs can be found. These are elements produced in factories before being assembled on site. The standard width of these hollow-core slab elements is around 1.20 m (Corgnati and Kindinis, 2007; Mohammad et al., 2014; Russell and Surendran, 2001; Winwood et al., 1994). At first, the cores were used to lessen the weight of the slab and to reduce production costs. Their reduced self-weight enabled them to provide long spans. They also offered the possibility of running electric cables or plumbing pipes within their cores. Soon, the cores began to be used to circulate air and avoid using false ceilings. The best documented of these systems is the TermoDeck® system. In a patent granted in 1971 for a “*Method and device for controlling the temperature in a premise*”, a hollow-core slab using throttles inside the channels was presented. The throttles could rotate and directed air to different parts of the channel walls. In (Wachenfeldt and Bell, 2013), however, it is reported that the early versions of the TermoDeck® installed in the 1980s often used under-sized ventilation, leading to discomfort.

Another kind of ventilated slabs are embedded-air-duct systems. Unlike hollow-core concrete slabs, embedded-air-duct systems are cast in situ. Ducts are simply laid on the formwork and then concrete is poured over them (see Figure 1). It is possible to vary the duct spacing, dimensions and shapes more freely than when using hollow-core concrete slab. Using ventilated slabs also avoids the need for false ceilings to cover the air duct networks. Thus, the ceiling height can be reduced, less material is required

and, in turn, cost savings can be made. In real estate terms, this means that, for a given height, more stories can be built when using this kind of system.



Figure 1: Photographs of the ventilation ducts before and during concrete pouring.

However, using air-based TABS impacts significantly heat transfer at the room scale compared to classical “all by air” systems. As illustrated in Figure 2, the outdoor air is prepared in a HVAC system prior to being blown through the slab. Part of the heat is transferred to the room by conduction through the slab and then by convection and radiation, \dot{Q}_T , and another part is blown into the room \dot{Q}_B . For a classical “all by air system”, the heat is provided by \dot{Q}_B only. On the one hand, the calculation of \dot{Q}_T is not straightforward because of the 3D nature of the heat transfer that takes place into the TABS. Besides, the slab that surrounds the pipes brings a significant thermal inertia, stressing the need for time-dependent model for estimating the heat transfer accurately. On the other hand, TABS system allow exchanging heat over a large surface, which helps in providing comfortable indoor conditions. Also, their strong thermal inertia can motivate the search of energy savings.

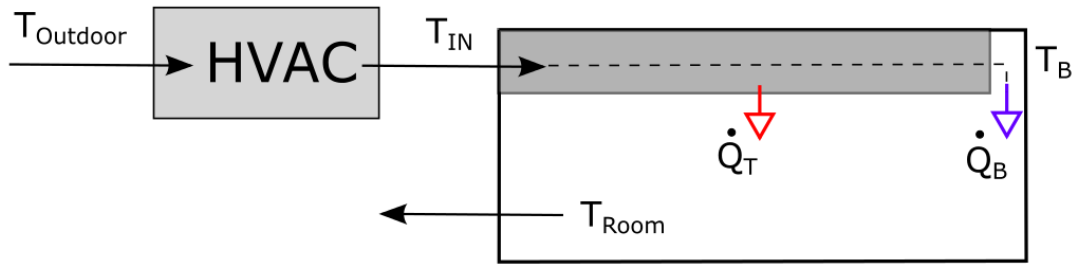


Figure 2: Integration of the ventilated slab at the room scale

The coupling of air-based systems with the room is more pronounced than water based systems, since the fluid is used for maintaining the indoor temperature within a comfortable range and for air renewal. While the physics of heat transfer within the slab does not differ significantly, embedded-air-ducts are facing other constraints than water based systems, which result in different designs. For example, the mass flow rate has to meet minimal flowrate requirements for hygiene purposes, and to remove indoor moisture. It is also limited in order to avoid undesirable effects that can occur at higher velocities (noise and draught). As a consequence, the design and/or analysis of air-based systems differs from that for water based systems.

Parametric studies of air-based TABS have already been proposed by other authors, giving some trends that are briefly summarized below.

1. The influence of the airflow rate was discussed in (Isanska-Cwiek, 2005; Winwood et al., 1997a, 1997b; Zmeureanu and Fazio, 1988). Logically, increasing the mass flow rate provides more heat (or cold for a cooling application) to the room. But a less intuitive finding was that increasing the mass flowrate reduced the fraction of the heating / cooling provided to the room by conduction through the slab (\dot{Q}_T in the present study) and increased the fraction of the heating / cooling provided to the room by direct air blowing (\dot{Q}_B in the present study).
2. The influence of the air path was discussed by (Barton et al., 2002; Winwood et al., 1997a) for the TermoDeck® system. They showed that increasing the number of activated cores decreases the temperature range at the outlet. In other words, a longer air path results in a higher quantity

of heat being exchanged with the slab. The same conclusion was obtained by Park and Krarti (2015), who found an asymptotic value for both heating and cooling modes.

3. Zmeureanu & Fazio (1988) varied the slab thickness from 10 to 20 cm, the cores being placed in the middle of the slab. They found that this parameter was meaningful at low ventilation rate but its influence diminished strongly as the airflow rate increased. A wider range of core depths was tested at low velocities (Park and Krarti, 2015) and illustrated the non-negligible influence of this parameter on the average heat transfer rate.
4. The high thermal inertia of concrete makes it interesting for TABS, yet this is offset by a rather low thermal conductivity. Winwood et al. (1997a) compared two concrete slabs for which thermal conductivity was increased by 10 and 20% by using aluminum seeding. Their results show that this has little or no impact on the outlet temperature. Recently, another approach based on the inclusion of Phase Change Materials (PCM) in mortars was proposed (Faheem et al., 2016; Guo et al., 2020) to increase the performance of the system.

The underlying difficulty in studying embedded air duct systems is that the computational cost is high, which is hardly compatible with an exhaustive study of their dynamic behavior. This has an adverse effect when it is necessary to deal with the control of TABS, which is crucial (Gwerder et al., 2008; Romani et al., 2016). For this reason, many authors have used lumped parameter models, which are able to reproduce the results obtained with detailed physics-based simulations with reasonable accuracy but at a much lower computational cost. Some examples can be found in (Fonseca, 2011; Gwerder et al., 2008; Weber and Jóhannesson, 2005) for water based systems. Fewer publications are available for air-based systems, with the notable exceptions of (Chen et al., 2013; Ren and Wright, 1998) in the framework of a hollow core concrete slab.

Different techniques are available to develop lumped models and are detailed in (Romani et al., 2016). A widespread technique used in thermal engineering relies on the thermal-electrical analogy to define an equivalent electrical circuit made of resistances and capacities. It has been successfully applied to

various building elements, including TABS (Gwerder et al., 2008; Viot et al., 2018; Weber and Jóhannesson, 2005). The RC circuit is generally set first, then the numerical values of its components are identified. While some RC circuits are now well known for some building elements, there are few results for ventilated slabs, except in a study (Ren and Wright, 1998) proposing a 4R2C model for a ventilated slab having its two faces exposed to different rooms. An acceptable accuracy of 0.9°C was obtained for the room temperature but higher discrepancies were observed during highly transient periods. The resistances were estimated from the geometrical description of the system while the thermal capacitances were adjusted to fit the experimental results.

A similar approach was proposed in the commercial software TRNSYS (TRANSSOLAR Energietechnik, 2017). While an analytical expression for an equivalent thermal resistance can be found, it is much harder to define equivalent thermal capacitances. This is one of the reason why advanced techniques are used to obtain equivalent capacitances, either from experimental results or from numerical simulations. However, these parameters are often case specific, hard to generalize, and their value is not always given.

Another technique relies on the use of transfer functions that define the relationship between one input and one output of the system by using mathematical transforms such as the Laplace transform. They can later be combined in a state space model that gives a linear combination of multiple outputs with multiple inputs. The advantage of this technique compared to the use of RC systems is that the expression of the lumped model does not necessarily have to be defined a priori. Its drawback is that it is not able to model nonlinear processes, such as in the case of variable mass flow rate. Some examples can be found (Chae and Strand, 2013; Strand and Baumgartner, 2005) of conduction transfer functions that were first developed for hydronic systems then modified to suit hollow core systems. A similar technique, named the frequency response, was used in (Chen et al., 2013) and allowed the thermal behavior of the system to be modeled in the frequency domain. However these approaches model only the dynamics of the slab and not that of the fluid. The fluid state equation needs to be

solved separately and its temperature distribution in the direction of the flow is considered stationary. Finally, other approaches are also available, such as a statistical model based on a significant amount of experimental data (Ferk1 and Jan Široký, 2010).

This paper aims to contribute to the understanding of the thermal behavior of embedded-air-duct systems at room scale. Specifically, we develop a methodology that utilize transfer functions that includes fluid dynamics, identify and validate the transfer functions using a detailed physical model, show how these transfer functions can be used to study the thermal performance at room scale, and draw conclusions regarding the influence of certain design parameters on this performance. The results will be set against the case of a conventional (non-ventilated) slab to highlight the benefits and the drawbacks of the ventilated slab, as well as the impact of the number and size of the ducts.

The paper is divided in three parts. The first part (section 2) presents the detailed finite element model of the ventilated slab. This detailed model will replace the real system for the next steps of the study. The second part (section 3) presents the method used to obtain the lumped parameters model of the ventilated slab out of the simulation data obtained with the detailed model. Finally the third part (section 4) integrates the lumped parameters model of the slab at the room level and studies the impact of the number of ducts and the flowrate on the thermal behavior of the room.

2. Physically based model of the ventilated slab

The objective of the physically based model is to generate data for the identification of the lumped model and its validation. It relies on a finite element commercial software (COMSOL) to solve heat transfer at the scale of the ventilated slab, while the heat transfers in the room and the HVAC system are ignored for now.

The description of the ventilated slab proposed here was inspired by a full scale commercial prototype built by Vinci in the inner suburbs of Paris. It was built in order to test the feasibility of the

GreenFloor® system prior to its commercialization. It was not intended to validate a heat transfer model however, and many elements necessary for this purpose are lacking (insufficient number of temperature and air flow measurements, unknown thermal properties for the concrete cast on site, uninsulated sidings and/or thermal bridges). Furthermore, some buildings equipped with the GreenFloor® system are already occupied. While they provide valuable information regarding the operation of the system, they are not fully instrumented and cannot be used for validation purposes.

The slab is 5 m long (L) and 0.22 m high (H), and the diameter of the embedded ducts d is 0.08 m. The ducts are placed regularly within the slab, their axes being spaced at $W = 0.45$ m apart. The system should be considered as a juxtaposition of some elementary parts, as highlighted in light grey in Figure 3. This design was selected to fit the requirements for classical offices and can be extended to a larger surface simply by adding elementary parts. In practice, the ducts are placed first and the concrete is poured over the whole surface at once, so that there is no physical separation between the different parts. The prototype and the system modeled here is a 20.25 m^2 slab that involves 9 ducts. Therefore, it can be broken down in 9 elementary parts.

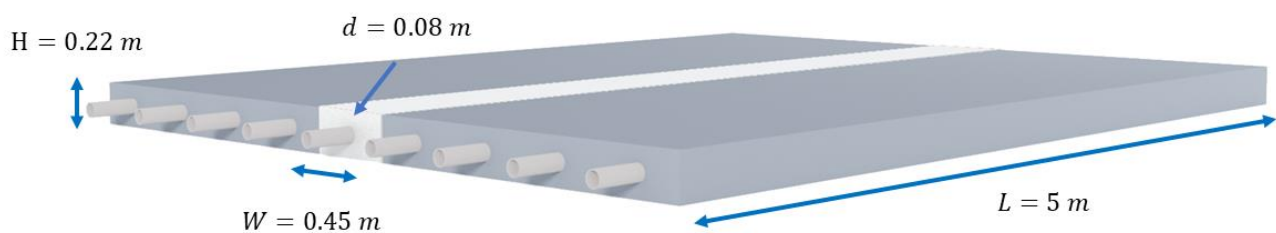


Figure 3: Ventilated slab dimensions and identification of an elementary part of the slab

Since the pipes are regularly spaced, there is no need to model the whole slab, provided that there is no heat transfer at the sides (the so-called thermal bridges). It is acknowledged, however, that the latter might be sizeable, as underlined by (Park and Krarti, 2015). Here, the modelling of the slab will focus on a single elementary part and, thanks to its symmetry, only half of that part will actually be modeled.

Two different domains have to be considered here: the heat transfer within the slab and heat transfers within the duct. For the slab, the classical heat equation in solids has to be solved.

$$\rho_c C_{p,c} \left(\frac{\partial T}{\partial t} \right) + \nabla(-k_c \nabla T) = 0 \quad (1)$$

The slab is homogeneous and made only of concrete. Classical thermal properties for concrete are considered: a density of $\rho_c = 2300 \text{ kg.m}^{-3}$, a specific heat capacity of $C_{p,c} = 880 \text{ J.kg}^{-1}.\text{K}^{-1}$, and a thermal conductivity of $k_c = 2.2 \text{ W.m}^{-1}.\text{K}^{-1}$.

For heat and mass transfer within the duct, a comprehensive approach would require solving the mass and momentum balances together with the heat balance. However, it would significantly burden the model for uncertain improvements in terms of accuracy. Here, we observe that the nature of heat transfer is not very different from those taking place in Earth to Air Heat Exchangers (EAHE). We propose to use the approach presented in (Estrada et al., 2018), where heat transfers in only one dimension are considered within the duct, while the pressure and velocity fields are not computed. For a single element defined by its length dx and its cross-section A , the heat balance yields:

$$\rho_a A \frac{dT}{dt} = -\dot{m}_a \frac{dT}{dx} + \frac{h_c p_d}{C_{p,a}} (T_w - T) \quad (2)$$

The air thermal properties are assumed constant and set to $\rho_a = 1.2 \text{ kg.m}^{-3}$ for the density and $C_{p,ca} = 1003 \text{ J.kg}^{-1}.\text{K}^{-1}$ for the specific heat capacity. The value for the convective heat transfer coefficient h_c is set as shown in Eqs. (3) to (5) (Holman, 1986).

$$h_c = \frac{k_a Nu_d}{d} \quad (3)$$

$$Nu_d = \frac{\left(\frac{f_D}{8} \right) (Re_d - 10^3) Pr}{1 + 12.7 \left(\frac{f_D}{8} \right)^{\frac{1}{2}} \left(Pr^{\frac{2}{3}} - 1 \right)} \quad (4)$$

$$f_D = (0.79 \ln(Re_d) - 1.64)^{-2} \quad (5)$$

where k_a is the thermal conductivity of air, set at $0.025 \text{ W.m}^{-1}.\text{K}^{-1}$.

The coupling between the slab and the duct is made through the wall temperature T_w , averaged over the perimeter of the duct cross-section for every position along its axis. In return, the convective heat flux computed within the pipe is used as a boundary condition for the slab.

As mentioned earlier, one of the strengths of the ventilated slab is to remove the need for false ceilings, providing more compact office buildings. However, it is unlikely that the rooms of two stories located one above the other will have the same demand at the same time, simply because, for example, the temperature set points might be different. Therefore, a ventilated slab cannot be used as a floor and a ceiling air-conditioning system simultaneously. As the cooling demand is significantly higher than the heating demand in modern offices, the ventilated slab should be used as a cooling ceiling in order to take advantage of natural convection. Consequently, the boundary conditions are the following:

1. The air temperature at the inlet of the duct T_{in} is fixed ;
2. There is no heat flux at the upper and side boundaries of the slab ;
3. A Robin boundary condition is applied to the lower part of the slab, namely by setting the temperature of the room, T_{Room} , and a heat transfer coefficient that accounts for both convective and radiative heat transfer. This coefficient is set to $8 \text{ W.m}^{-2}.\text{K}^{-1}$.

A constant mass flow rate is used in this study. While it is acknowledged that variable air flow systems are now widespread, it was anticipated that this technique would not suit the purpose of this study very well. To a certain extent, varying the airflow rate would result in bypassing the thermal inertia of the system and addressing indoor comfort mostly by the air blown into the room. Another reason for considering a constant airflow rate is that it facilitates the identification of the lumped model. In this study, we propose to use a $300 \text{ m}^3.\text{h}^{-1}$ airflow rate, which leads to an air renewal of approximately 6 ach. This value is higher than the requirement of the French regulations (1 ach in this case). However, early tests performed with the commercial prototype showed that it was adequate to achieve

comfortable indoor conditions in most situations. Nevertheless, the influence of the airflow rate will be illustrated later by repeating the computational work for 100 and 500 $\text{m}^3 \cdot \text{h}^{-1}$.

The problem was solved by using commercial finite element software (COMSOL). The meshing of the slab was refined close to the pipe and to the lower surface. It was defined on the side at the inlet of the pipe (450 surface elements), then swept along the pipe direction by using a distribution containing 50 elements, the size of which increased progressively toward this direction as shown in Figure 4. A mesh distribution of 100 elements was used for the duct in 1D. The final mesh contained 22500 elements for the slab. Mesh sensitivity was tested by doubling the number of elements, which resulted in only 1% difference in the air temperature at the outlet of the duct or in the heat flux at the bottom of the slab. Finally, the problem was found to be sensitive to the time-step tolerance, which was set to 10^{-3} .

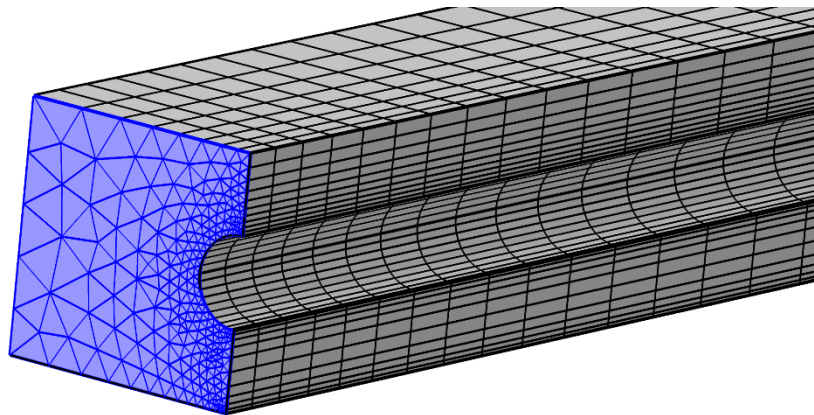


Figure 4: Meshing of the slab surface at the inlet of the pipe (highlighted in blue) and swept mesh in the direction of the pipe axis.

In order not to stick to a single configuration of the ventilated slab, other geometries were tested by changing the number of ducts (N_D). To ease comparison, three constraints were imposed. Both the total mass flow rate and the volume occupied by the ducts within the slab remained the same. Also, the height (H) and length (L) of the slab remained constant for all cases. In consequence, the air velocity remained the same for all cases. This allowed four other systems to be defined, whose parameters are

briefly summarized in Table 1. Finally, the air flow rate was modified only for the geometry used as a reference case, leading to a total of seven different systems.

Table 1: Parameters used for all the ventilated slabs

N_D	3	6	9*	12	15	9	9
d (10^{-3} m)	139	98	80	69	62	80	80
W (10^{-2} m)	135	68	45	34	27	45	45
\dot{m}_a ($\text{kg}\cdot\text{s}^{-1}$) per duct	$3.33 \cdot 10^{-2}$	$1.66 \cdot 10^{-2}$	$1.11 \cdot 10^{-2}$	$8.33 \cdot 10^{-3}$	$6.66 \cdot 10^{-3}$	$5.53 \cdot 10^{-3}$	$1.85 \cdot 10^{-2}$
h_c ($\text{W}\cdot\text{m}^{-2}\cdot\text{k}^{-1}$)	7.8	8.4	8.8	9.0	9.2	3.2	13.1
* Reference case							

The methodology presented in this paper was set and validated for the reference case first, then applied to all other cases.

3. Lumped model of the ventilated slabs

In this section, the input and the output of the transfer functions will be defined first, then the identification methodology will be described. The behavior of the seven different systems will be compared by means of Bode magnitude plots. Finally, the accuracy of the lumped (state space) model will be discussed.

3.1. Definition of the inputs and outputs

A transfer function gives the relationship between an input and one output of the system. When the system has several inputs and outputs, the number of transfer functions is equal to the product of the number of inputs and the number of outputs. The first step consists in defining the inputs of the ventilated slab and proposing relevant outputs. Our objective is to obtain a lumped model that is suitable for computing the heat balance at the room scale, which, at steady state, is:

$$\dot{Q}_{HVAC} + \dot{Q}_L = 0 \quad (6)$$

Here, \dot{Q}_L is the total of the heat loads of the room. It can be broken down into several terms to represent the heat flux through the envelope and the ones resulting from the use of appliances for example. However, it has an impact on the indoor temperature, T_{Room} , rather than on the ventilated slab itself. For this reason, it will not be included in the definition of the transfer functions.

\dot{Q}_{HVAC} is the heat flux provided to the room by an HVAC system by means of a ventilated slab. Assuming that the pressure of the room is higher than outdoors and in the corridor, the mass flow rate blowing into and out of the room are the same, so \dot{Q}_{HVAC} can be defined by:

$$\dot{Q}_{HVAC} = \dot{m}_a C_{p,a} T_{in} - \dot{m}_a C_{p,a} T_{Room} \quad (7)$$

Now, considering that the ventilated slab is a subsystem of the room, this heat flux can also be broken down into three terms as follows:

$$\dot{Q}_{HVAC} = \dot{Q}_T + \dot{Q}_B + \dot{Q}_S \quad (8)$$

where \dot{Q}_T is the heat flux transmitted to the room by conduction through the slab, \dot{Q}_S is the heat flux stored within the slab (null at steady state) and \dot{Q}_B is the heat flux blown into the room, given by:

$$\dot{Q}_B = \dot{m}_a C_{p,a} (T_B - T_{Room}) \quad (9)$$

From the slab's perspective, it appears that the room temperature, T_{room} , and the inlet temperature, T_{in} , are the only two exogenous inputs. The heat flux stored in the slab is not useful for computing the heat balance at the room scale, so \dot{Q}_T and \dot{Q}_B were chosen as the two outputs. As a result, four transfer functions have to be identified for the lumped model. A dimensionless form is preferred, giving:

$$\begin{aligned} F_{T,T_{in}} &= \frac{\dot{Q}_T}{\dot{m}_a C_{p,a} T_{in}} & F_{T,T_{Room}} &= \frac{\dot{Q}_T}{-\dot{m}_a C_{p,a} T_{Room}} \\ F_{B,T_{in}} &= \frac{\dot{Q}_B}{\dot{m}_a C_{p,a} T_{in}} & F_{B,T_{Room}} &= \frac{\dot{Q}_B}{-\dot{m}_a C_{p,a} T_{Room}} \end{aligned} \quad (10)$$

One of the drawbacks of the transfer functions in the case of multi-input/multi-output systems is that the functions have to be combined linearly to compute the outputs. The definition proposed in (10) enables us to write:

$$\begin{aligned}\dot{Q}_T &= \dot{m}_a C_{p,a} (F_{T,T_{in}} T_{in} - F_{T,T_{Room}} T_{Room}) \\ \dot{Q}_B &= \dot{m}_a C_{p,a} (F_{B,T_{in}} T_{in} - F_{B,T_{Room}} T_{Room})\end{aligned}\tag{11}$$

This will be finally achieved later, by transforming the transfer functions into a state-space representation.

Next, a general expression of a transfer function can be given as follows:

$$F(s) = K \frac{\prod \left(\frac{1}{z_i} s + 1 \right)}{\prod \left(\frac{1}{p_j} s + 1 \right)} e^{-\tau_0 s}\tag{12}$$

where s is the Laplace variable, K is the static gain, z_i are the zeros, p_j are the poles and τ_0 is the time delay. The objective is to propose a model with minimum coefficients and good accuracy.

Some constraints on the above parameters can be deduced from the physics of heat transfer. The static gain of the transfer function is the ratio of one output to one input at steady state. Here, the static gain for $F_{T,T_{in}}$ and $F_{B,T_{in}}$ represents the fraction of the heat flux provided to the slab that is transmitted or blown to the room, respectively. At steady state, there is no heat flux stored within the slab, which leads to:

$$K_{F_{T,T_{in}}} + K_{F_{B,T_{in}}} = 1\tag{13}$$

The same holds when the room temperature varies, and:

$$\begin{aligned}K_{F_{T,T_{in}}} &= K_{F_{T,T_{Room}}} \\ K_{F_{B,T_{in}}} &= K_{F_{B,T_{Room}}}\end{aligned}\tag{14}$$

In the frequency domain, the transfer function can also be analyzed as the ratio of the output to the input amplitudes depending on the frequency (f), the latter being included in the definition of the Laplace variable. For rapid periodic variations of room temperature, the heat flux is adsorbed and released by a thin layer of concrete in contact with the room air, having no impact on the wall temperature, T_w , in the duct. In this case, the amplitude of the air temperature at the outlet of the duct (denoted \widehat{T}_B) is null, leading to:

$$\lim_{f \rightarrow \infty} F_{B, T_{Room}} = 1 - \frac{\widehat{T}_B}{\widehat{T}_{Room}} = 1 \quad (15)$$

The same thing happens when the inlet temperature T_{in} follows rapid periodic variations. The temperature in the vicinity of the duct varies but the temperature at the surface of the ceiling remains constant, leading to:

$$\lim_{f \rightarrow \infty} F_{T, T_{in}} = 0 \quad (16)$$

3.2. Identification of the transfer functions

Early tests, not presented here, were achieved by using harmonic excitations of the inputs in order to estimate the Bode diagram of the four transfer functions. This indicated that three transfer functions would be correctly modeled by using 2 zeros and 2 poles. The Bode diagram was noticeably different for $F_{T, T_{in}}$, which should be modeled with only 1 zero and 2 poles. Finally, a 2.7 s delay (τ_0) was identified for the transfer functions used to model the heat flux blown to the room ($F_{B, T_{in}}$ and $F_{B, T_{room}}$). Physically, this corresponds to the time taken by the air to move through the length of the pipe. However, this time delay is very much lower than the other time constants, including the ones used for control in buildings. It was therefore ignored.

Identification of the coefficients relied on the use of dedicated Matlab functions. Based on the least squares method, it retrieves the coefficients that fit the time series used as a reference, which was obtained with the physical model. One strong limitation with this method is that it requires the use of

a constant time step for the whole time series. The frequency range that has to be explored thus gives the minimum number of points of the time series (N_{min}) as follows:

$$\begin{aligned}\Delta t_{max} &= \frac{1}{2 f_{max}} \\ t_{min} &= \frac{1}{f_{min}} \\ N_{min} &= \frac{t_{min}}{\Delta t_{max}} = 2 \frac{f_{max}}{f_{min}}\end{aligned}\tag{17}$$

Here, Δt_{max} is the simulation time step (which should satisfy the Shannon frequency) and t_{min} is the simulation time (which should represent at least one period of the smallest frequency). Early tests showed that the frequency range of typical excitations of the system under study, and thus to be used to plot the Bode diagram, was $[10^{-8}: 10^{-2}]$ Hz, leading to the need to generate at least $2 \cdot 10^6$ points. As this far exceeds the capacities of the software (limited to approximately $4 \cdot 10^4$ points, not to mention the computational time), it was decided to split the identification process in two steps. First, the inputs were generated in the low frequency range ($[10^{-8}: 10^{-5}]$ Hz) by using a chirp signal, providing a signal with a frequency that increased smoothly against time. Next, a Pseudo Random Binary Sequence (PRBS) was used to explore the high frequency range ($[10^{-6}: 10^{-2}]$ Hz). As it produces step-like variations of the input, it covers a wider range of frequencies and imitates sudden temperature variations that are likely to happen in reality, when a device is turned on for example. Thus, for the first frequency range, we needed only $N_{min} = 2 \cdot 10^3$ points and, for the second one, $N_{min} = 2 \cdot 10^4$ points.

The reference values for the outputs were obtained by simulating the system in COMSOL with the above input profiles. Based on this response, the identification can be broken down into three steps.

Briefly:

1. A steady state simulation was run first to identify the value of the static gain, which was adjusted to fit (13).
2. The time series at low frequency was then used next to identify the poles and zeros situated roughly in this frequency range, the static gain being fixed. Each transfer function had one pole and one zero in this range.
3. The time series at high frequency was used next to identify the other poles and zeros (if any) in order to improve the response fidelity, the other parameters being fixed. Here again, each transfer function had one additional pole and one additional zero, except for $F_{T,T_{in}}$, which had one additional pole only. They were slightly adjusted afterwards to meet the requirements of (15).

The final expression for $F_{B,Room}$ is given in (18) as an example.

$$F_{B,Room}(p) = 0.607 \frac{(7.46 \cdot 10^4 s + 1)(1.16 \cdot 10^4 s + 1)}{(4.72 \cdot 10^4 s + 1)(1.11 \cdot 10^4 s + 1)} \quad (18)$$

Note that the second pole and zero are very close to each other. The improvement of the transfer function obtained by adding these two coefficients is, in fact, negligible, and this equation could be reduced. However, as these coefficients bring a physical meaning at high frequencies and as they do not significantly burden the model, they were kept for this transfer function. The identification of $F_{T,Room}$ and $F_{B,T_{in}}$ led to similar conclusions. The high frequency poles/zeros identified were, however, outside the bandwidth of the excitation signals and were therefore removed. The values of the coefficients for all the transfer functions are summarized in Table 4, which has been placed in the appendix for the sake of clarity.

The output responses obtained with the physical model, which stands as the reference here, are compared with those obtained with the transfer function $F_{B,T_{in}}$ in Figure 5 for illustration purposes. The magnitude of the error lies roughly within the range of $\pm 4\%$. The model accuracy will be discussed in greater detail in section 3.5.

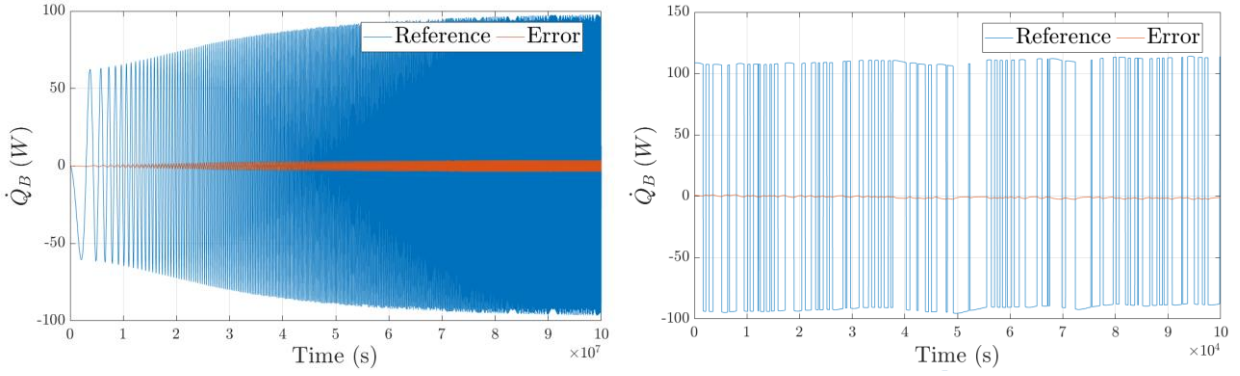


Figure 5: Heat flux, Q_B , blown into the room when T_{Room} varies and error obtained with the transfer function. Results obtained with a chirp signal can be seen on the left and a PRBS signal on the right.

3.3. Influence of the number of ducts

The methodology presented in the previous section was applied to the other four configurations of the system, leading to a total of 20 transfer functions. They are compared by means of the Bode magnitude plots presented in Figure 6 and Figure 7. For the sake of clarity, the Bode phase plots are not presented.

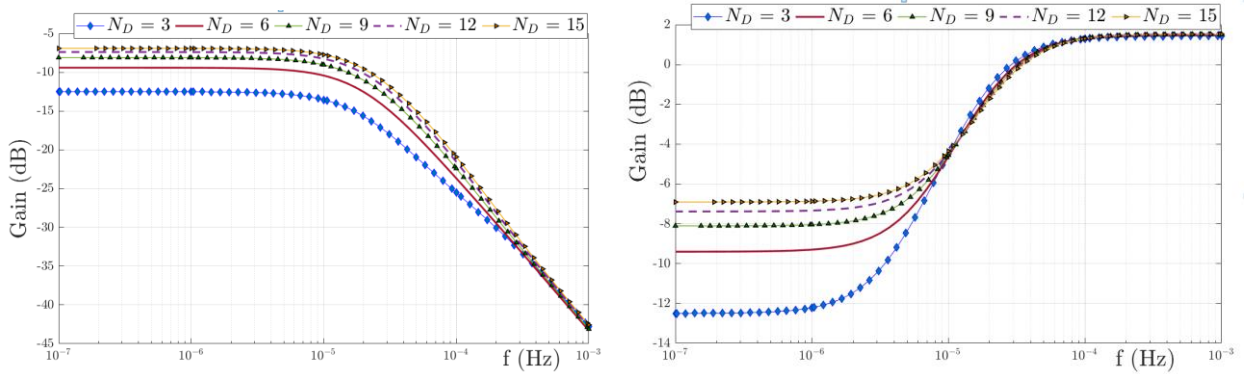


Figure 6: Bode magnitude plot for $F_{T,Tin}$ (left) and $F_{T,TRoom}$ (right) when the number of ducts, N_D , varies.

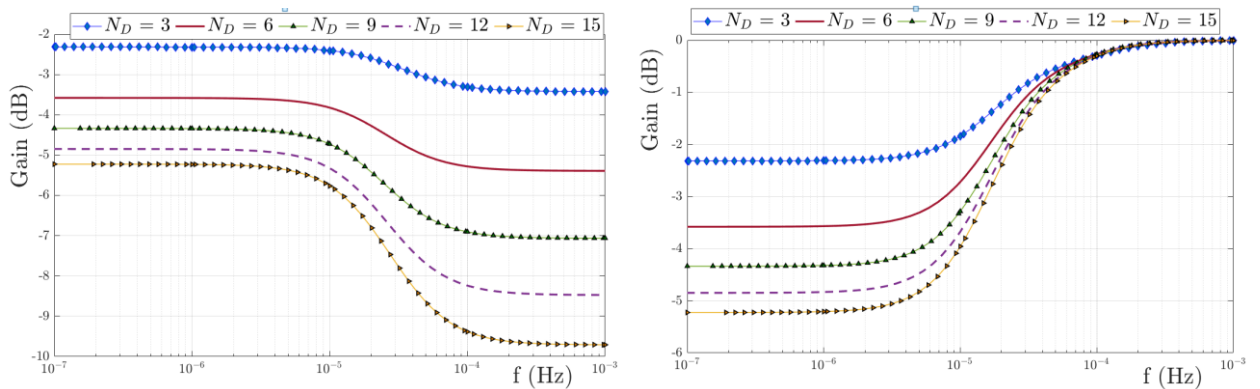


Figure 7: Bode magnitude plot for $F_{B,Tin}$ (left) and $F_{B,TRoom}$ (right) when the number of ducts, N_D , varies.

First of all, it appears that the magnitude remains constant for frequencies outside the $[10^{-6}; 10^{-3}]$ Hz range, with the notable exception of $F_{T,Tin}$. The static gain corresponds to the magnitude obtained at low frequencies and is discussed below. For three ducts ($N_D = 3$), a larger fraction of the heat provided by the HVAC system is blown into the room (76%) than transmitted through the slab (24%) in the steady state. Under the constraint of a constant volume occupied by the ducts, increasing the number of ducts results in a more balanced distribution of the heat fluxes (54% and 46% respectively for fifteen ducts).

Second, the shape of the Bode magnitude plot is approximately the same for $F_{B,TRoom}$ and $F_{T,TRoom}$, i.e. for the transfer functions related to the room temperature. The influence of N_D at low frequencies was already debated when discussing the static gain but it is noteworthy that it has no influence at high frequencies. Therefore, discussion of the influence of N_D can be based on the static gain and the transfer functions related to the inlet temperature T_{in} only.

Next, the Bode magnitude plot for $F_{T,Tin}$ is similar to a low pass filter. Its cutoff frequency is approximately $2 \cdot 10^{-5}$ Hz, this value being only slightly dependent on N_D ($\pm 7\%$ compared to the reference case). In other words, the time constant of this filter is approximately 2.2 h. Moreover, at high frequencies, the gain is roughly identical for all N_D . The heat flux transmitted through the slab will not be significantly modified for rapid variations (shorter than 2.6 minutes) of the inlet temperature T_{in} , because of its thermal inertia. On the other hand, a constant heat flux would be obtained roughly 6.6 h after a step variation of T_{in} (under the assumption of a constant room temperature).

Considering $F_{B,Tin}$, the system behaves differently. Rapid variations of the inlet temperature, T_{in} , will be passed on to the heat flux blown into the room, but with a smaller amplitude than for lower frequencies, because of the heat transfer with the slab. Comparing this Bode plot with the one obtained for $F_{T,Tin}$ reveals the influence of the heat flux stored and released by the slab (\dot{Q}_S in equation (8)). Its

influence starts at roughly $7 \cdot 10^{-6}$ Hz, and increases progressively with the frequency, up to an asymptotic value that is reached for frequencies higher than approximately $5 \cdot 10^{-4}$ Hz. Note that the influence of N_D is considerable here, as increasing the number of ducts will increase \dot{Q}_S . For fluctuations with periods lower than half an hour, the ratio of the amplitude of T_B to the amplitude of T_{in} is 66% for $N_D = 3$, but drops to 30% for $N_D = 15$. This means that 34% (70% for $N_D = 15$) of the variation of the heat flux provided at the inlet is stored and released successively, smoothing the temperature variation of the air blown into the room.

3.4. Influence of the mass flow rate at the scale of the ventilated slab

The influence of the mass flow rate was tested only for the ventilated slab equipped with nine ducts. The mass flow rate was changed to 100 and 500 $\text{m}^3 \cdot \text{h}^{-1}$, values that are representative of an air renewal of 2 and 10 ACH for the room located below the ventilated slab. The Bode magnitude plots of the transfer functions are presented in Figure 8 and Figure 9. The values of the coefficients are given in Table 5 in the appendix.

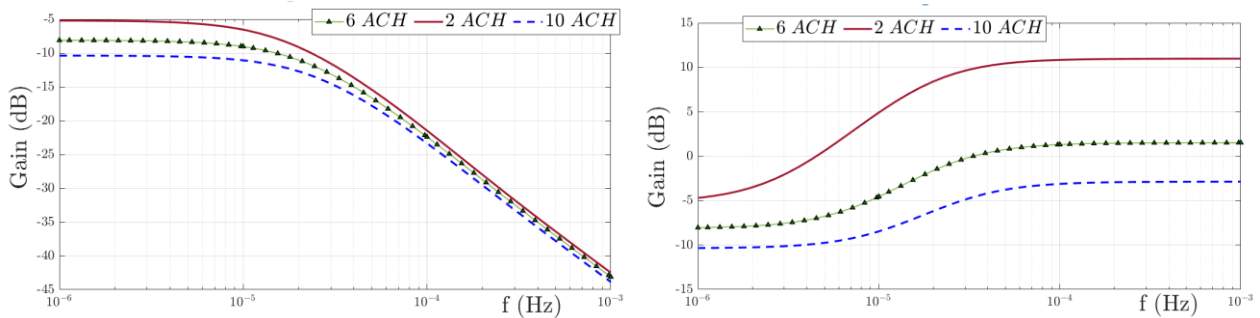


Figure 8: Bode magnitude plot for $F_{T,Tin}$ (left) and $F_{T,TRoom}$ (right) for different air change rates.

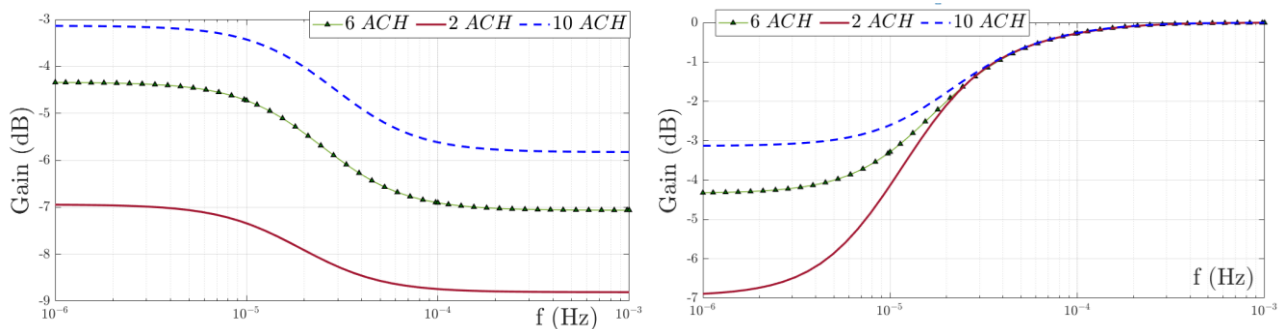


Figure 9: Bode magnitude plot for $F_{B,Tin}$ (left) and $F_{B,TRoom}$ (right) for different air change rates.

First, it can be observed that the time constants tend to increase when the airflow rate is lowered, and conversely. This means that the system behaves more slowly for a lower air change rate, which is equivalent to a system that provides more inertia. Considering the transfer functions related to the input temperature T_{in} , the time constants vary slightly over the range [-35 : 35]%. The variation is more pronounced for the transfer functions related to the room temperature (up to ([-170 : 75]% for $F_{T,TRoom}$).

Second, the influence of the mass flow rate on the static gain is the most obvious. Reducing the mass flow rate increases the fraction of the heat flux transmitted through the slab and diminishes the fraction blown into the room, so that they reach 55% and 45%, respectively, for 2 ACH. The opposite happens when the mass flow rate increases to 10 ACH, leading to 70% of the heat flux being blown into the room at steady state. However, increasing the mass flow rate also means that the cooling power provided to the ventilated slab is more important. It is interesting to observe that, despite a lower fraction being transmitted to the room by conduction, the net heat flux would be the highest for 10 ACH under the assumption of steady state. This is summarized in Table 2, where the numerical values have been calculated assuming a temperature difference of 12°C between the inlet and the room.

Table 2: Comparison of the heat flux obtained at steady state for different air flow rates.

<i>ACH</i>	$\frac{\dot{Q}_T}{\dot{Q}_{HVAC}}$	$\frac{\dot{Q}_B}{\dot{Q}_{HVAC}}$	\dot{Q}_{HVAC}^* (kW)	\dot{Q}_T^* (kW)
2	55.0%	45.0%	0.40	0.22
6	39.3%	60.7%	1.21	0.47
10	30.3%	69.7%	2.01	0.61

* Obtained under the assumption that $(T_{in} - T_{Room}) = 12^\circ\text{C}$

The sizing of most “all-by-air” systems for cooling relies on the limit imposed on the temperature difference between the air blown into the room and the room itself. For the occupants’ comfort, this difference should not be greater than 12°C. Then, the air flow rate is determined so that the system is able to cope with the internal heat loads. Using a ventilated slab brings an alternative, as the temperature of the air blown into the room, T_B , differs from that of the air blown into the ventilated

slab, T_{in} . In other words, the HVAC system could provide a lower airflow rate at a lower temperature. However, this technique has to face two major drawbacks: first, the temperature of the surface of the ceiling has to remain higher than the indoor dew point temperature. Second, this logic assumes a steady state, so \dot{Q}_S is zero. Given the time constants of the system, however, it is likely that the steady state will hardly be reached in practice, stressing the need for dynamic simulations. These will be obtained through the use of a state space model in this paper.

3.5. State space model and its validation

The four transfer functions can be combined in a state space model as follows:

$$\begin{cases} \dot{x} = Ax + Bu \\ y = Cx + Du \end{cases} \quad (19)$$

where u and y are column vectors containing the inputs and the outputs, respectively, of the transfer functions.

$$\begin{aligned} u &= [\dot{m}C_{p,a}T_{in}(t) \quad -\dot{m}C_{p,a}T_{Room}(t)]^T \\ y &= [\dot{Q}_T(t) \quad \dot{Q}_S(t)]^T \end{aligned} \quad (20)$$

x is a column vector containing the state variables. A , B , C and D are matrices that contain the parameters of the system. They can be related to the coefficients of the transfer function by using a partial fraction decomposition. As this would not add value to this study, it will not be detailed here and the values of the coefficients in the four matrices are not presented.

The sizes of these matrices depend directly on the number of poles of the transfer functions (for matrix A), as well as the number of inputs (for matrix B) and the number of outputs (for matrix C). The dimension of the state space model proposed here is 6. To validate the identified state space model, a new simulation was run with the physically based model (Comsol model) but with an excitation different from the one used for identification. The idea of doing this was to test the robustness of the identified model. Here, we propose to use on site measurements of T_{in} and T_{Room} taken during one

month at mid-season in an occupied building (see Figure 10), as they provide realistic temperature ranges and variations. On the real TABS, the control was achieved by varying the air flowrate and using a simple on/off control for heating or cooling. As a consequence, the inlet temperature (T_{in}) variations were rapid and in large magnitude. In the system studied in the present paper, temperature variations at the inlet are expected to be smoother because of the use of a constant flowrate. Nevertheless, using the *in situ* measurements will result in a validation test that is more demanding. Conversely, the room temperature remained within a narrow range.

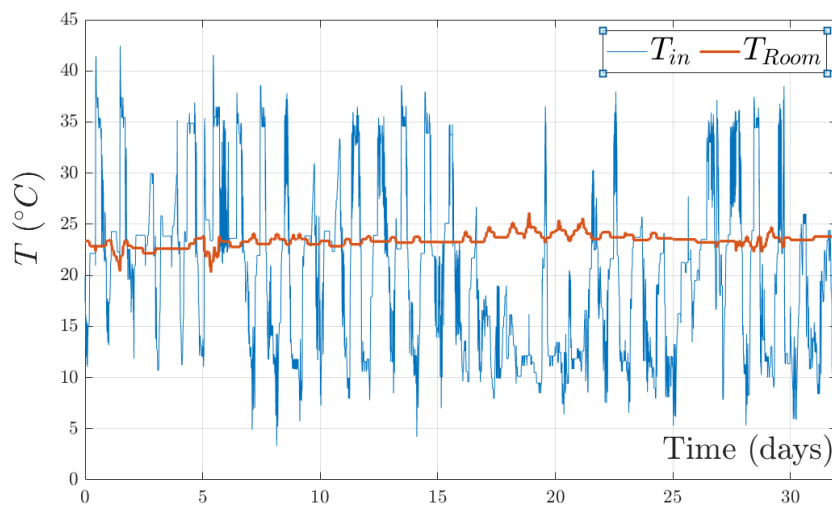


Figure 10: Inputs used to validate the state space model.

The results are compared in Figure 11 for the reference case ($N_D = 9$), where positive values are used when heating is provided to the room and negative values for cooling. Here, it should be recalled that the transfer functions and the state space model were developed for an elementary part of the slab containing only one duct. The heat fluxes have to be multiplied by 9 to be representative of a 20.25 m² office, leading to an air-conditioning power magnitude of approximately ± 1.5 kW.

The mean error obtained with the state space model is lower than 0.03 W and 95% of the error remains within a ± 2 W and ± 4 W interval, for the transmitted and blown heat fluxes respectively. This represents a relative error of $\pm 10\%$ with respect to the average heat flux in both cases. Overall, it confirms that the average behavior is captured with very good accuracy, while higher errors may occur

punctually when quick variations happen. They result from a small lag and do not lead to a significant bias. This validation test was repeated for the other ventilated slab models and led to similar conclusions.

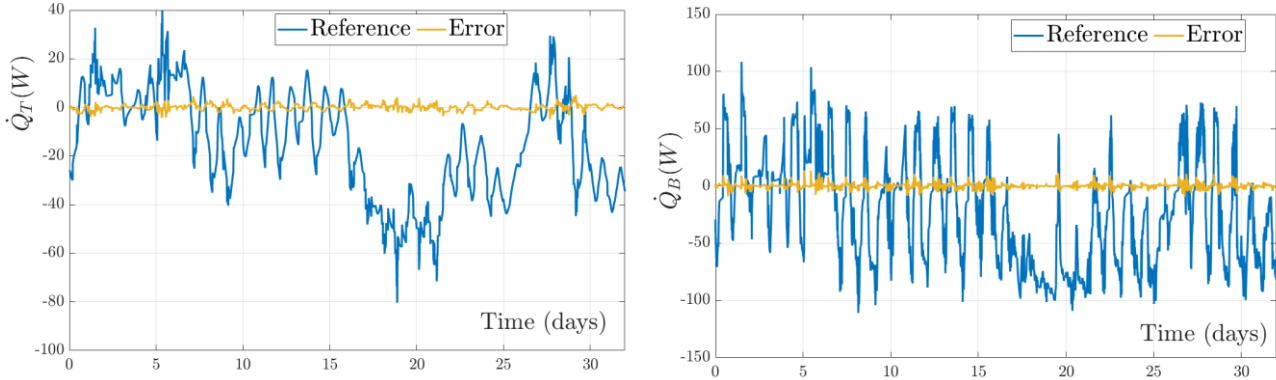


Figure 11: Comparison of the results obtained with the physical and the lumped models for $N_D = 9$. Heat flux transmitted to the room through the slab (left) and blown into the room (right).

Finally, let us mention that the computational time required to run the validation test with the physical model exceeded 17 h on a machine equipped with eight 2.2 GHz processors and with 100 Go RAM. The results were obtained with the lumped model in less than one second, illustrating its relevancy.

4. Influence of the ventilated slab on the heat balance of the room: a test case

The objective of this section is to illustrate the behavior of the ventilated slabs in the context of a typical tertiary building. Therefore, we move from the scale of the ventilated slab to that of the room. The test case is designed to be representative of typical office conditions. Simple boundary conditions and control laws are considered in order to highlight the influence of the number of ducts and of the air change rate.

4.1. Test case description

The test case is based on a 20.25 m² room, typical for multi-story office buildings and directly inspired from the room used for testing the prototype of the ventilated slab. For the sake of simplicity, the room is assumed to be at an intermediate level, so the ground and roof have no influence. It has a single

exterior wall and the ventilated slab is taken to be installed on its ceiling. The floor is not modelled, nor are the partition walls (see Figure 12). The HVAC system is still not modelled, yet T_{in} represents the temperature at its outlet and differs from $T_{Outdoor}$.

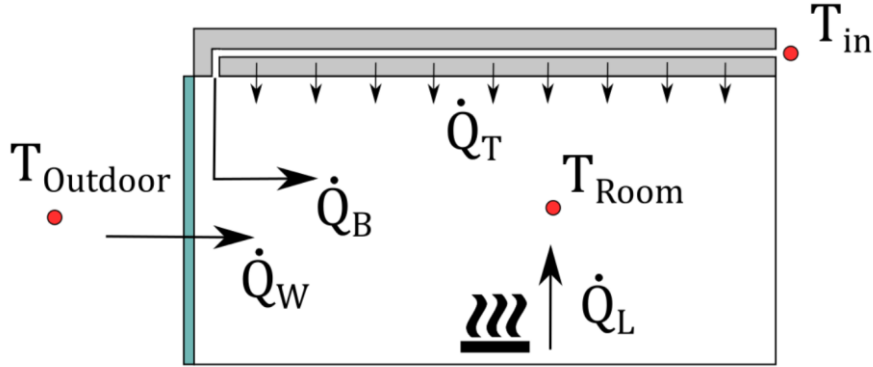


Figure 12: Scheme of the heat balance at the room scale

The heat balance at the room scale gives:

$$\dot{Q}_T + \dot{Q}_B + \dot{Q}_L + \dot{Q}_W - (\rho_A V_{Room} + I A_f) c_{p,A} \frac{\partial T_{Room}}{\partial t} = 0 \quad (21)$$

where I is a coefficient used to take the thermal inertia of the indoor furniture into account. Its value is set at 40 kg.m^{-2} , which is representative of an office with medium furnishing according to (Johra and Heiselberg, 2017).

Heat transfer through the wall is evaluated by considering a glazed wall, a common feature of modern high-rise offices. As its mass is rather small compared to the GreenFloor®, its thermal inertia is neglected and the heat transfer can be evaluated as follows:

$$\dot{Q}_W = U A_W (T_{Outdoor} - T_{Room}) \quad (22)$$

where U is an overall heat transfer coefficient set at $1.5 \text{ W.m}^{-2}.\text{K}^{-1}$, A_w stands for the vertical wall surface (10.125 m^2) and $T_{Outdoor}$ is the temperature outdoors.

The climatic conditions of Montpellier, France, were selected and are representative of a Mediterranean climate. Since it was harder to design the system for cooling purposes, a 4 day long hot period was selected for this test case (see Figure 13). The internal heat loads \dot{Q}_L are modeled very

simply as a rectangular type signal. Its magnitude is 50 W per square meter of floor area from 8h to 18h, and set to zero otherwise. It is acknowledged that the reality is far more complex, but a simple model for the heat loads was preferred in order to ease the comparison between the ventilated slabs studied here.

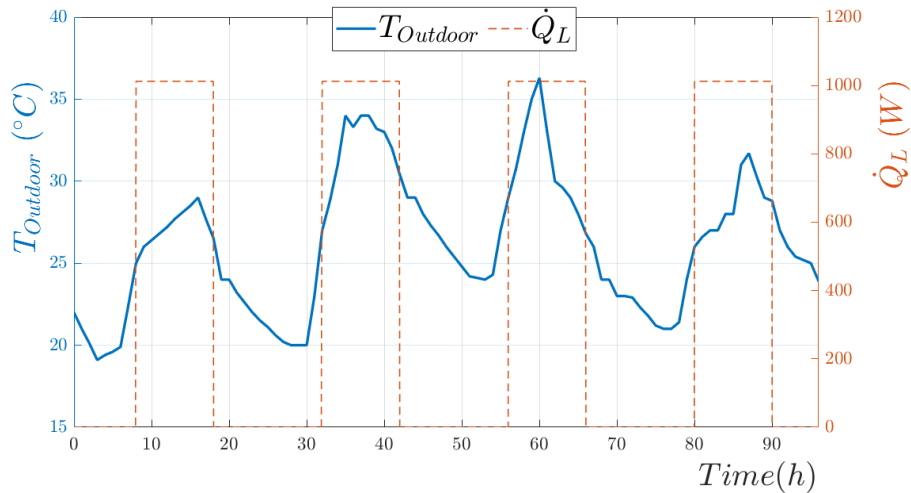


Figure 13: Outdoor conditions and heat loads used for the test case

The temperature at the inlet of the slab T_{in} was set according to a simple control law, namely a fixed temperature set point combined with hysteresis. Although this technique is simple, it is still quite common for systems in building applications, even with TABS (Sourbron et al., 2009). Here, the indoor set point was fixed at 22 ± 2 °C and T_{in} was set at 10 °C for cooling, 22 °C otherwise, as illustrated in Figure 14. Air that enters in the TABS at T_{in} is conditioned by the HVAC system. During some short periods, the outdoor air is cooler than the indoor set point. Assuming the demand to be for cooling only, a test was added to prevent the outdoor fresh air from being heated before being blown into the ventilated slab. This was achieved by setting the inlet temperature to the outdoor temperature when the latter was lower than the value obtained with the control law. For the sake of clarity, the HVAC was not modeled and an ideal system was considered instead. By this, we mean that the response of the HVAC system was assumed to be immediate and exact.

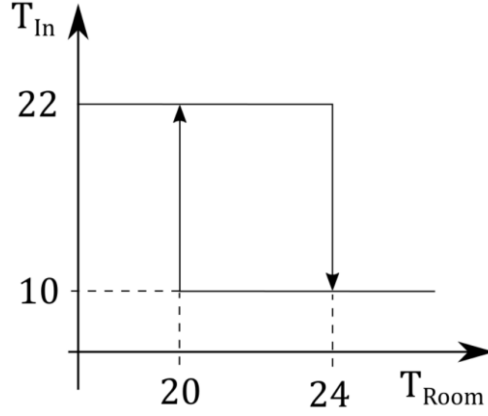


Figure 14: Control law used for setting the temperature at the inlet of the ventilated slab.

An adaptive time step technique was implemented in order to verify that dividing the time step by two did not result in a difference higher than 10^{-3} °C on T_{Room} . All the simulations were initialized by considering that both the room and the slab were at a homogeneous temperature (22 °C).

4.2. Non-ventilated slab model

For comparison, the thermal behavior of the room was assessed when a classical all by air system (referred later as Non Ventilated Slab (NVS)) was used instead of a ventilated slab. As the heat transfers were much simpler than for the ventilated slab, a classical 1D finite difference model with an implicit time scheme was preferred to a state space model. The model was written with Matlab. It was validated by comparing the results with the analytical solution for conductive heat transfer within a semi-infinite solid, the upper face of which ($z = 0$) was subjected to a sinusoidal variation (Ozgener et al., 2013). The temperature profile along the z direction, the z axis being downward, was given at any time by:

$$T(z, t) = \overline{T}_u - \widehat{T}_u e^{-\sqrt{\frac{\pi}{\alpha T}} z} \cos\left(\frac{2\pi}{P}(t - \tau) - \sqrt{\frac{\pi}{\alpha P}} z\right) \quad (23)$$

The average upper temperature \overline{T}_u and its amplitude \widehat{T}_u were set to 20 and 5 °C, respectively. The period, P , was set to 1 year and the delay, τ , to zero. The thermal diffusivity, α , was set using the thermal properties of concrete already mentioned in this paper. A 30 m deep slab was modeled for 4

years in order to obtain results that were independent of the initial conditions. The number of nodes and the time step were tuned accordingly. The highest discrepancy was 7.10^{-3} °C, for a time selected at random.

4.3. Results obtained for the reference case

The values computed for T_{Room} and T_{in} are plotted in Figure 15 for the reference case ($N_D = 9$ and a total air renewal of 6 ACH). This system was able to maintain the room temperature between 20 and 24 °C during the four days. Overall, the room temperature increased sharply in the morning, because of the internal heat loads, until it reached 24 °C. Then, the temperature at the inlet of the ventilated slab decreased to 10 °C, which helped to maintain the room temperature between 23 and 24 °C until 6 p.m. Note that T_{in} remained constant during this whole period, meaning that the HVAC system had to run continuously to cool the room. At 6 p.m., the indoor temperature decreased suddenly as the heat loads were set to zero. The temperature set point of the HVAC system remained the same for one more hour, then the room temperature reached 20 °C and the temperature set point changed to 22 °C. As this reference case was assumed to take place in summer, the HVAC system still had to provide cooling to reach such a temperature, unless the outdoor air was cooler, in which case it was insufflated directly into the ventilated slab. This technique is very simple and might not make best use of the thermal inertia of the ventilated slab. Still, the room temperature increased slightly and remained lower than 22 °C until next morning, which is the target temperature for comfort. While more realistic techniques could be implemented, those presented ease the analysis of the system and its comparison with different values of N_D and of the air change rate.

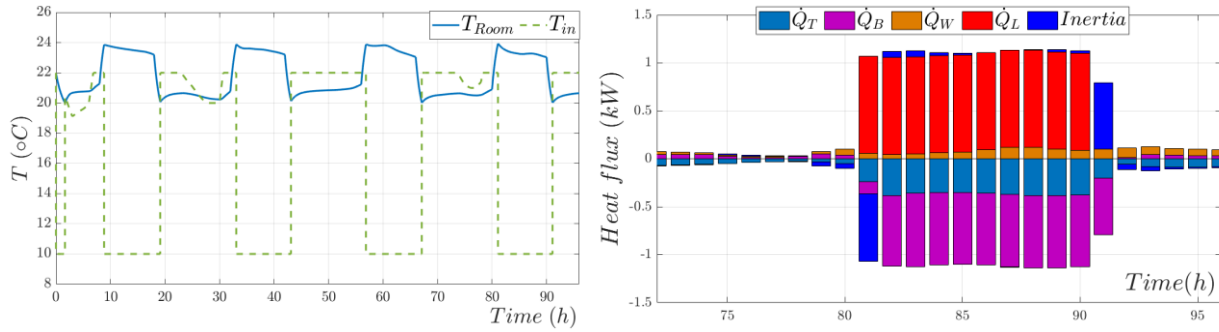


Figure 15: Room and inlet temperatures obtained for the reference case (left) and heat balance at the room scale for the fourth day (right).

Next, the heat fluxes used to compute the heat balance at the room scale according to (21) were hour-averaged and are plotted in Figure 15 for the fourth day only. A positive value means that the room is receiving a positive heat flux or that the room temperature is decreasing (because of the negative sign on the term for indoor inertia in (21)).

From 9 a.m. to 6 p.m., the HVAC system provided cooling continuously in order to mitigate the internal heat loads. The mean cooling power was -1.12 kW, approximately one third of which was supplied to the room through the slab and the rest by the blown air. These ratios varied little over this whole period. Note that they are close to the static gains ratio (40% and 60% for $N_D = 9$).

When the heat loads were off, the magnitude of the heat fluxes at the room scale dropped to 0.1 kW. The temperature at the inlet, T_{in} , was slightly above the room temperature, T_{Room} , because of the control law used here. Consequently, the heat flux blown into the room, \dot{Q}_B , was positive while the heat flux exchanged with the slab, \dot{Q}_T , was negative, meaning that the slab was still cooling the room. It is acknowledged that more energy-efficient control laws could have been proposed. Nevertheless, indoor conditions remained comfortable during the whole period.

4.4. Influence of the number of ducts and of the mass flow rate

The previous simulation work was repeated for the same scenario but with different numbers of ducts and different air change rates. The results are plotted in Figure 16 and Figure 17, respectively.

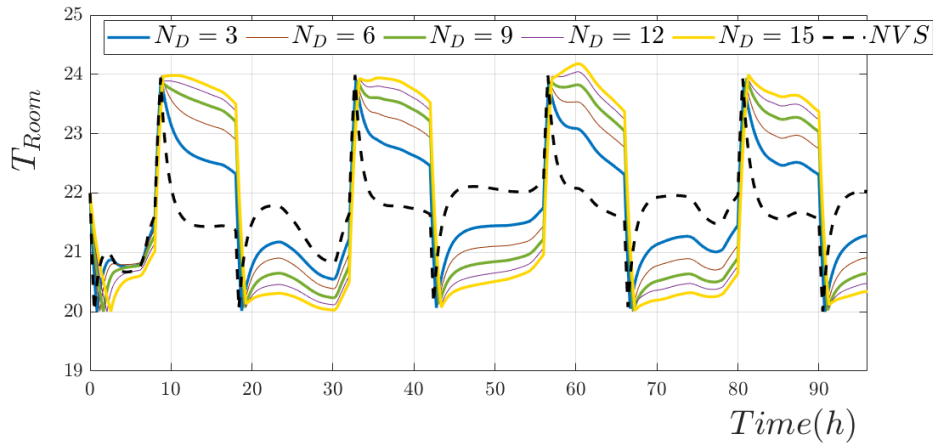


Figure 16: Room temperature obtained with different number of ducts N_D and with the non-ventilated slab (NVS) under a constant air change rate (6 ACH).

The heat balance at the room scale was slightly affected by the number of ducts N_D since the time and duration for cooling were approximately the same. The indoor temperature, T_{Room} , remained within the targeted range for all systems. However, it can be observed that increasing the number of ducts led to less variable indoor temperatures, regardless of whether the heat loads were on or off. Also, the indoor temperature remained closer to the threshold values (20 and 24 °C) when the number of ducts increased. This is consistent with the previous conclusions that the amount of heat transmitted to the room increases with the number of ducts. This favors thermal inertia and consequently smooths indoor temperature variations. The non-ventilated slab had the same overall dimensions as the other systems, but led to faster indoor temperature variation when the inlet temperature, T_{in} , changed. The result was a slightly cooler indoor environment during the day and a hotter one during the night. The comparison with the results obtained with the ventilated slab illustrates the increased thermal capacity brought by the slab. Another interesting result is that comfortable indoor conditions were achieved by considering a ventilated slab combined with a simple control law. Unlike the hydronic TABS, a significant fraction of the heat flux blown into the slab was transmitted to the room almost instantaneously. On one hand, it is harder to take full advantage of the thermal inertia of the slab but, on the other hand, it seemed easier to provide a fast response to indoor temperature changes. It is foreseen that this may ease the

control of the system and avoid uncomfortable indoor conditions caused by a slow response to unforeseen indoor temperature variations.

The influence of the mass flow rate was more pronounced than with varying N_D , as depicted by Figure 17. While the room temperature was approximately the same at 8 a.m. for all systems, significant differences were appearing as soon as the heat loads were on.

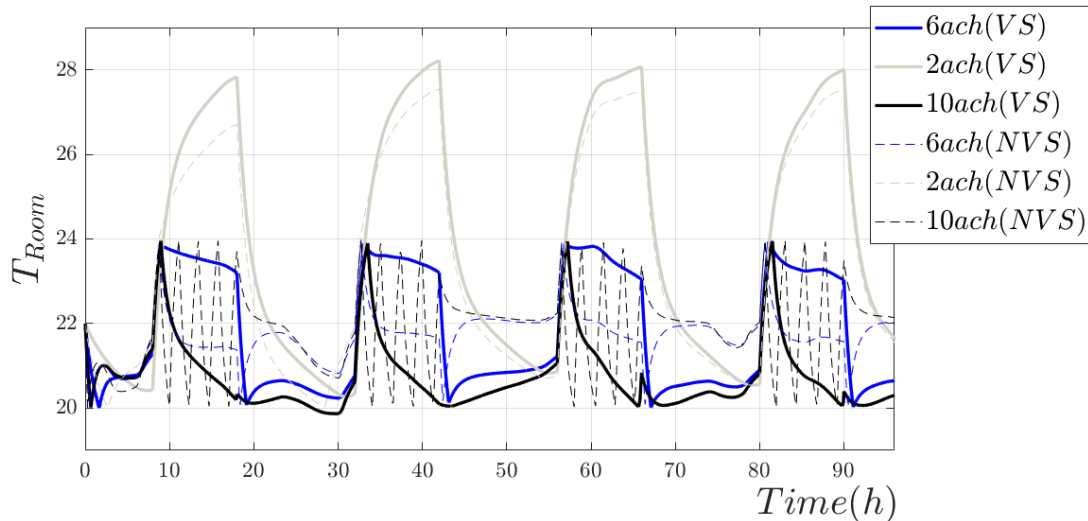


Figure 17: Room temperature obtained with different air change rates for a ventilated slab equipped with 9 ducts (VS) and a non-ventilated slab (NVS).

For the lowest air flow rate, the indoor temperature could not be maintained below 24 °C. In fact, it never reached 20 °C during the four days, meaning that the HVAC system provided cooling continuously. Despite the thermal inertia of the slab, it can be concluded that the cooling power provided to the room was insufficient to meet the indoor temperature requirements when the air flow rate was set at 2 ACH. Only minimal temperature differences were observed between the VS and the NVS systems, which was not expected. As mentioned above, the heat flux transmitted through the slab was higher at lower air flow rates, stressing the difference with a conventional system (here, an NVS). However, this is not evident here. The reason for the difference lies in the mode of heat transfer, a ventilated slab providing a more diffuse heat flux through the ceiling compared to an all-by-air system, which might have an impact on indoor comfort. However, the results obtained here show that,

considering the high internal heat loads, the heat balance at the room scale was not greatly affected. This statement tends to mitigate the idea that a low air flow rate should be used to take advantage of a ventilated slab.

Increasing the mass flow rate to 10 ACH led to cooler indoor temperature when the heat loads are on. For the VS, however, it can be observed that the HVAC system had to supply cooling almost continuously from 8 a.m. to 6 p.m., which is very similar to what was obtained with 6 ACH. On the other hand, the indoor temperature obtained with the NVS was more scattered during the day. As the indoor temperature varies much faster, it reached the lower and the upper thresholds several times a day, leading the HVAC system to be turned on and off repeatedly. This hardly ever happened with the VS at the same air change rate, because of its additional thermal capacity.

To investigate a little further, the cooling demand was estimated with (24). The results were divided by the value obtained for the reference case and are presented in Table 3.

$$E = \int \dot{m}_a C_{p,a} (T_{Outdoor} - T_{in}) dt \quad (24)$$

Table 3: Relative cooling demand for the 6 different cases

Air flow rate	6 ach	2 ach	10 ach
VS	1*	0.63	1.47
NVS	0.95	0.57	1.08

* Reference case

The results show the strong influence of the air change rate on the cooling demand. It could be roughly approximated by a linear relationship for the VS: varying the air change rate by 1 ACH led to an increase of about 10% in the energy consumption for this test case. However, for the non-ventilated slab, this statement was no longer valid. For 10 ACH, the lower threshold was reached several times during the day. In consequence, the HVAC provided less cooling for a while and the total energy consumption was increased only slightly compared to the reference case, for the operating conditions

used here. For the other cases, the energy consumption was slightly lower than that obtained with a ventilated slab. The reason is that, because of the increased inertia of the VS, there was still a cooling demand at the end of the day, while there were no more heat loads. The opposite happened in the morning but the time shift was smaller, leading to a higher cooling demand with VS than with NVS. Obviously, the control law proposed here is usable with the NVS but it does not take advantage of the additional thermal inertia of the ventilated slab and leads to higher energy consumption.

Overall, these results show that N_D has a limited impact on the room temperature, yet increasing the number of ducts is desirable in order to promote better indoor temperature stability. This conclusion is important for practitioners as it means that the number of ducts is a parameter of lesser significance that can be adjusted to fit on site constraints. On the other hand, the airflow rate has a significant impact. While a low airflow rate favors heat transfer by conduction through the slab, there was little difference on the heat balance of the room compared with a non-ventilated slab; the need to supply cooling to the room in order to balance the heat loads still existed. This need defines a minimum air flow rate that is required to achieve comfortable indoor temperatures. Increasing the airflow rate will help this objective to be met but at the cost of a higher energy consumption. At the same time, the influence of the control law is likely to be greater at higher airflow rates, and it should be tuned carefully in order to avoid extra energy consumption.

4.5. Discussion

The methodology used here to obtain a lumped model for the ventilated slab was found to be adequate for a fairly wide range of geometries and airflow rates. It strongly diminishes the computational time for the heat transfer, allowing coupling with a room model. For the test case proposed here, the computational time was approximately 1.5 s for a simulation period of one day.

There is a clear need to define an adequate airflow rate and a relevant command law for the ventilated slab to provide comfortable indoor conditions while being energy efficient. First of all, the simulation

should be run for a longer period than four days in order to offer a wider range of outdoor conditions. As the heat loads were found to have a significant impact on the indoor heat balance, they should be modeled in greater detail. For example, they could include solar gains, which are time and orientation specific. Also, a stochastic occupancy schedule could be used to be more realistic, as exemplified by (Bui et al., 2019), among others. Finally, the HVAC system has to be modeled in order to give a more accurate estimation of the energy consumption. It could include an energy recovery system on the exhaust flow for example, which appears relevant as soon as the airflow rate increases. Moreover, the cooling unit should be modeled so as to include a heat pump and its coefficient of performance (COP). This would be relevant to test night-cooling strategies, as the COP increases during the night, when the outdoor air is cooler.

The influence of the control law on the energy consumption was underlined by (Sourbron et al., 2009) in the framework of a hydronic TABS, with a control law similar to the one used here. In practice, such basic control laws are very common because they are easy to set up. Although the results presented in this paper are limited to a narrow range of boundary conditions, they indicate that using the same control law as for a non-ventilated slab did not result in major changes in terms of comfort and energy consumption, as long as the air change rate was appropriate. This is an interesting result as it questions the idea that a complex control strategy must necessarily be used with TABS, and could help ventilated slabs to become more widely accepted.

Advanced control strategies, such as Model Predictive Control (MPC), are now mature and fulfill the needs for reducing building energy consumption well (Ma et al., 2012). One such strategy has been successfully applied to hydronic systems (Feng et al., 2015). It is recognized that this technique might not be easy to implement on an existing HVAC system, as a retrofit may be required to deal with the computational cost of this technique. On the other hand, it might bring interesting insight that would allow a simple control law to be optimized. Further research should consider this kind of option in order to explore a broad range of control strategies.

5. Conclusions

The thermal behavior of ventilated slabs is 3D and strongly time-dependent. Consequently, it makes the use of a detailed physically based model tedious when the aim is to model their behavior at room scale. This study relies on a lumped model based on the identification of transfer functions for constant airflow rate systems. They were combined into a state space model, which was able to obtain the heat fluxes with good accuracy ($< 10\%$ error for instantaneous heat fluxes, and almost no deviation over a long-term simulation) at a much lower computational cost.

The methodology was applied repeatedly for different air flow rates and numbers of ducts, under the constraint of the volume occupied within the slab being constant. Increasing the number of ducts led to a higher fraction of heat flux transmitted through the slab, which is desirable. It also increased the amount of energy that was stored and released within the slab for rapid temperature variations at the inlet of the slab. Reducing the airflow rate increased the share of the heat flux transmitted through the slab even more, yet it also led to a system that behaved more slowly. While increasing the mass flow rate diminished the fraction transmitted through the slab, it was observed that the total heat flux transmitted increased, which is noteworthy.

Then, the study moved to room scale. A test case was proposed in order to further understand how the ventilated slabs influence the heat balance. A four day long hot period was selected and a simple yet realistic control law was proposed. Increasing the number of ducts helped to promote better indoor temperature stability, but the impact was slight. The mass flow rate, on the other hand, appeared to be crucial. For a low air flow rate, the indoor temperature exhibited almost no difference with a conventional slab, thus questioning the benefits obtained with a ventilated slab. The differences were more pronounced at higher air flow rates (6 and 10 ACH), both on the indoor temperature and for the cooling demand. Although for 6 ACH the cooling demand remained quite similar, the indoor temperature was more stable during the occupied/unoccupied periods with the ventilated slab,

indicating that a simple control law can be efficient for a ventilated slab. For 10 ACH, however, the cooling demand was found to increase dramatically compared to a non-ventilated slab. This result underlines the need to tailor a control law specifically for the ventilated slab, based on a larger set of simulations at the room scale. Further research should focus on this issue, taking advantage of the short computational time provided by the lumped model.

6. References

- Antonopoulos, K.A., Tzivanidis, C., 1997. Numerical solution of unsteady three-dimensional heat transfer during space cooling using ceiling-embedded piping. *Energy* 22, 59–67.
- Barton, P., Beggs, C.B., Sleight, P.A., 2002. A theoretical study of the thermal performance of the TermoDeck hollow core slab system. *Appl. Therm. Eng.* 22, 1485–1499.
- Basaran, T., Ilken, Z., 1998. Thermal analysis of the heating system of the Small Bath in ancient Phaselis. *Energy Build.* 27, 1–11. [https://doi.org/10.1016/S0378-7788\(97\)00013-3](https://doi.org/10.1016/S0378-7788(97)00013-3)
- Bean, R., Olesen, B.W., Kim, K.W., 2010. History of Radiant Heating and Cooling. *ASHRAE J.* 40–50.
- Bui, R., Labat, M., Lorente, S., 2019. Impact of the occupancy scenario on the hygrothermal performance of a room. *Build. Environ.* 160, 106178. <https://doi.org/10.1016/j.buildenv.2019.106178>
- Chae, Y.T., Strand, R.K., 2013. Modeling ventilated slab systems using a hollow core slab: Implementation in a whole building energy simulation program. *Energy Build.* 57, 165–175. <https://doi.org/10.1016/j.enbuild.2012.10.036>
- Chen, Y., Athienitis, A.K., Galal, K.E., 2013. Frequency domain and finite difference modeling of ventilated concrete slabs and comparison with field measurements: Part 1, modeling methodology. *Int. J. Heat Mass Transf.* 66, 948–956. <https://doi.org/10.1016/j.ijheatmasstransfer.2013.05.076>
- Corgnati, S.P., Kindinis, A., 2007. Thermal mass activation by hollow core slab coupled with night ventilation to reduce summer cooling loads. *Build. Environ.* 42, 3285–3297. <https://doi.org/10.1016/j.buildenv.2006.08.018>
- Estrada, E., Labat, M., Lorente, S., Rocha, L.A.O., 2018. The impact of latent heat exchanges on the design of earth air heat exchangers. *Appl. Therm. Eng.* 129, 306–317. <https://doi.org/10.1016/j.applthermaleng.2017.10.007>
- Evelyn, J., 1691. *Kalendarium Hortense: or, The Gardeners Almanac, Directing what he is to do Monthly throughout the Year. And What Fruits and Flowers are in Prime*, 8th ed. R Chiswell in St Paul's Churchyard, T Sawbridge in Little-Britain and R Bentley in Russell-Street in Covent Garden, London.
- Faheem, A., Ranzi, G., Fiorito, F., Lei, C., 2016. A numerical study on the thermal performance of night ventilated hollow core slabs cast with micro-encapsulated PCM concrete. *Energy Build.* 127, 892–906. <https://doi.org/10.1016/j.enbuild.2016.06.014>

- Feng, J. (Dove), Chuang, F., Borrelli, F., Bauman, F., 2015. Model predictive control of radiant slab systems with evaporative cooling sources. *Energy Build.* 87, 199–210. <https://doi.org/10.1016/j.enbuild.2014.11.037>
- Ferkl, L., Jan Široký, 2010. Ceiling radiant cooling: Comparison of ARMAX and subspace identification modelling methods. *Build. Environ.* 45, 205–212. <https://doi.org/10.1016/j.buildenv.2009.06.004>
- Fonseca, N., 2011. Experimental study of thermal condition in a room with hydronic cooling radiant surfaces. *Int. J. Refrig.* 34, 686–695. <https://doi.org/10.1016/j.ijrefrig.2010.12.019>
- Guo, J., Jiang, Y., Wang, Y., Zou, B., 2020. Thermal storage and thermal management properties of a novel ventilated mortar block integrated with phase change material for floor heating: an experimental study. *Energy Convers. Manag.* 205, 112288. <https://doi.org/10.1016/j.enconman.2019.112288>
- Gwerder, M., Lehmann, B., Tödtli, J., Dorer, V., Renggli, F., 2008. Control of thermally-activated building systems (TABS). *Appl. Energy* 85, 565–581. <https://doi.org/10.1016/j.apenergy.2007.08.001>
- Haden, G.N., 1924. *Activities*. G.N. Haden & sons Ltd.
- Holman, J.P., 1986. *Heat Transfer*. McGraw-Hill.
- Isanska-Cwiek, A., 2005. Experimental and CFD research on the thermal performance of the air cooled slab system. Presented at the Ninth International IBPSA Conference, Montréal, Canada, pp. 443–450.
- Johra, H., Heiselberg, P., 2017. Influence of internal thermal mass on the indoor thermal dynamics and integration of phase change materials in furniture for building energy storage: A review. *Renew. Sustain. Energy Rev.* 69, 19–32. <https://doi.org/10.1016/j.rser.2016.11.145>
- Koschenz, M., Dorer, V., 1999. Interaction of an air system with concrete core conditioning. *Energy Build.* 30, 139–145.
- Ma, Y., Kelman, A., Daly, A., Borelli, F., 2012. Predictive Control for Energy Efficient Buildings with Thermal Storage: Modeling, Stimulation, and Experiments. *IEEE Control Syst.* 32, 44–64. <https://doi.org/10.1109/MCS.2011.2172532>
- Mohammad, W.S., Murtadha, T.K., Ahmed, K.A., 2014. Using TermoDeck System for Pre-Cooling/Heating to Control the Building Inside Conditions. *Al-Khwarizmi Eng. J.* 10, 13–24.
- Ozgener, O., Ozgener, L., Tester, J.W., 2013. A practical approach to predict soil temperature variations for geothermal (ground) heat exchangers applications. *Int. J. Heat Mass Transf.* 62, 473–480. <https://doi.org/10.1016/j.ijheatmasstransfer.2013.03.031>
- Park, B., Krarti, M., 2015. Development of a simulation analysis environment for ventilated slab systems. *Appl. Therm. Eng.* 87, 66–78. <https://doi.org/10.1016/j.applthermaleng.2015.04.065>
- Ren, M.J., Wright, J.A., 1998. A ventilated slab thermal storage system model. *Build. Environ.* 33, 43–52. [https://doi.org/10.1016/S0360-1323\(97\)00030-9](https://doi.org/10.1016/S0360-1323(97)00030-9)
- Rhee, K.-N., Olesen, B.W., Kim, K.W., 2017. Ten questions about radiant heating and cooling systems. *Build. Environ.* 112, 367–381. <https://doi.org/10.1016/j.buildenv.2016.11.030>
- Romaní, J., de Gracia, A., Cabeza, L.F., 2016. Simulation and control of thermally activated building systems (TABS). *Energy Build.* 127, 22–42. <https://doi.org/10.1016/j.enbuild.2016.05.057>

- Russell, M.B., Surendran, P.N., 2001. Influence of active heat sinks on fabric thermal storage in building mass. *Appl. Energy* 70, 17–33.
- Sourbron, M., De Herdt, R., Van Reet, T., Van Passel, W., Baelmans, M., Helsen, L., 2009. Efficiently produced heat and cold is squandered by inappropriate control strategies: A case study. *Energy Build.* 41, 1091–1098. <https://doi.org/10.1016/j.enbuild.2009.05.015>
- Strand, R.K., Baumgartner, K.T., 2005. Modeling radiant heating and cooling systems: integration with a whole-building simulation program. *Energy Build.* 37, 389–397. <https://doi.org/10.1016/j.enbuild.2004.07.009>
- Thébert, Y., 2003. Thermes romains d’Afrique du Nord et leur contexte méditerranéen, Bibliothèque des Écoles françaises d’Athènes et de Rome. Publications de l’École française de Rome, Rome.
- TRANSSOLAR Energietechnik, G., 2017. TRNSYS 18 - a TRAnsient SYstem Simulation program - Volume 5 Multizone Building modeling with Type56 and TRNBuild [WWW Document].
- Viot, H., Sempey, A., Mora, L., Batsale, J.C., Malvestio, J., 2018. Model predictive control of a thermally activated building system to improve energy management of an experimental building: Part I—Modeling and measurements. *Energy Build.* 172, 94–103. <https://doi.org/10.1016/j.enbuild.2018.04.055>
- Wachenfeldt, B.J., Bell, D., 2013. Building Integrated Energy Systems in Smart Energy Efficient Buildings – A State-of-the Art (PROJECT REPORT No. STF22 A04503). SINTEF Civil and Environmental Engineering Architecture and Building Technology, Trondheim, Norway.
- Weber, T., Jóhannesson, G., 2005. An optimized RC-network for thermally activated building components. *Build. Environ.* 40, 1–14. <https://doi.org/10.1016/j.buildenv.2004.04.012>
- Winwood, R., Benstead, R., Edwards, R., 1997a. Advanced fabric energy storage II: Computational fluid dynamics modelling. *Build. Serv. Eng. Res. Technol.* 18, 7–16.
- Winwood, R., Benstead, R., Edwards, R., 1997b. Advanced fabric energy storage III: theoretical analysis and whole-building simulation. *Build. Serv. Eng. Res. Technol.* 18, 17–24.
- Winwood, R., Benstead, R., Edwards, R., Letherman, K.M., 1994. Building fabric thermal storage: Use of computational fluid dynamics for modelling. *Build. Serv. Eng. Res. Technol.* 15, 171–178. <https://doi.org/10.1177/014362449401500308>
- Zhang, L., Liu, X.-H., Jiang, Y., 2012. Simplified calculation for cooling/heating capacity, surface temperature distribution of radiant floor. *Energy Build.* 55, 397–404. <https://doi.org/10.1016/j.enbuild.2012.08.026>
- Zhuang, Z., Li, Y., Chen, B., Guo, J., 2009. Chinese kang as a domestic heating system in rural northern China—A review. *Energy Build.* 41, 111–119. <https://doi.org/10.1016/j.enbuild.2008.07.013>
- Zmeureanu, R., Fazio, P., 1988. Thermal performance of a hollow core concrete floor system for passive cooling. *Build. Environ.* 23, 243–252.

7. Acknowledgments

The authors would like to thank IC Entreprises for supporting this research work and Guillaume Rabut for sharing his experience and expertise related to Vinci's GreenFloor® system. M. Cezard is funded by ICE under the CIFRE grant n°2017/1790.

8. Appendix

Table 4 : Coefficient obtained for the transfer functions with different N_D values (6 ach)

Transfer function	Form	N_D	K	z_1	z_2	p_1	p_2
$F_{T,T_{in}}$	$K \frac{(z_1 s + 1)}{(p_1 s + 1)(p_2 s + 1)}$	3	0.236	9.76E+03	-	5.24E+04	6.03E+03
		6	0.338	7.08E+03	-	5.13E+04	6.84E+03
		9	0.393	5.99E+03	-	4.86E+04	6.96E+03
		12	0.428	5.44E+03	-	4.67E+04	6.93E+03
		15	0.452	5.03E+03	-	4.54E+04	6.78E+03
$F_{T,T_{Room}}$	$K \frac{(z_1 s + 1)}{(p_1 s + 1)}$	3	0.236	2.69E+05	-	5.38E+04	-
		6	0.338	1.63E+05	-	4.66E+04	-
		9	0.393	1.30E+05	-	4.29E+04	-
		12	0.428	1.14E+05	-	4.07E+04	-
		15	0.452	1.04E+05	-	3.93E+04	-
$F_{B,T_{in}}$	$K \frac{(z_1 s + 1)}{(p_1 s + 1)}$	3	0.764	2.68E+04	-	3.04E+04	-
		6	0.662	3.52E+04	-	4.34E+04	-
		9	0.607	3.46E+04	-	4.74E+04	-
		12	0.572	3.13E+04	-	4.75E+04	-
		15	0.548	2.81E+04	-	4.72E+04	-
$F_{B,T_{Room}}$	$K \frac{(z_1 s + 1)(z_2 s + 1)}{(p_1 s + 1)(p_2 s + 1)}$	3	0.764	6.45E+04	8.35E+03	5.15E+04	7.99E+03
		6	0.662	7.23E+04	1.05E+04	5.00E+04	1.00E+04
		9	0.607	7.46E+04	1.16E+04	4.72E+04	1.11E+04
		12	0.572	7.61E+04	1.18E+04	4.54E+04	1.13E+04
		15	0.548	7.74E+04	1.22E+04	4.44E+04	1.17E+04

Table 5 : Coefficients obtained for the transfer functions with different airflow rates ($N_D = 9$)

Transfer function	Form	ACH	K	z_1	z_2	p_1	p_2
$F_{T,T_{in}}$	$K \frac{(z_1 s + 1)}{(p_1 s + 1)(p_2 s + 1)}$	6	0.393	5.99E+03	-	4.86E+04	6.96E+03
		2	0.550	6.29E+03	-	6.03E+04	7.68E+03
		10	0.303	5.69E+03	-	4.20E+04	6.43E+03
$F_{T,T_{Room}}$	$K \frac{(z_1 s + 1)}{(p_1 s + 1)}$	6	0.393	1.30E+05	-	4.29E+04	-
		2	0.550	3.50E+05	-	5.45E+04	-
		10	0.303	8.72E+04	-	3.68E+04	-
$F_{B,T_{in}}$	$K \frac{(z_1 s + 1)}{(p_1 s + 1)}$	6	0.607	3.46E+04	-	4.74E+04	-
		2	0.450	4.68E+04	-	5.81E+04	-
		10	0.697	2.97E+04	-	4.05E+04	-
$F_{B,T_{Room}}$	$K \frac{(z_1 s + 1)(z_2 s + 1)}{(p_1 s + 1)(p_2 s + 1)}$	6	0.607	7.46E+04	1.16E+04	4.72E+04	1.11E+04
		2	0.450	1.26E+05	1.18E+04	5.92E+04	1.12E+04
		10	0.697	5.62E+04	1.14E+04	4.07E+04	1.10E+04